High-throughput computational prediction of the cost of carbon capture using mixed matrix membranes

Journal:	*Energy & Environmental Science*
Manuscript ID	EE-ART-09-2018-002582.R1
Article Type:	Paper
Date Submitted by the Author:	15-Oct-2018
Complete List of Authors:	Budhathoki, Samir; National Energy Technology Laboratory Ajayi, Olukayode; National Energy Technology Laboratory Steckel, Janice; National Energy Technology Laboratory Wilmer, Christopher; University of Pittsburgh, Chemical and Petroleum Engineering

SCHOLARONE™
Manuscripts

Journal Name

ROYAL SOCIETY
OF CHEMISTRY

ARTICLE TYPE

High-throughput computational prediction of the cost of carbon capture using mixed matrix membranes†

Samir Budhathoki,[a,b] Olukayode Ajayi,[a] Janice A. Steckel,[a] and Christopher E. Wilmer[a,c]

Polymeric membranes are being studied for their potential use in post-combustion carbon capture on the premise that they could dramatically lower costs relative to mature technologies available today. Mixed matrix membranes (MMMs) are advanced materials formed by combining polymers with inorganic particles. Using metal-organic frameworks (MOFs) as the inorganic particles has been shown to improve selectivity and permeability over pure polymers. We have carried out high-throughput atomistic simulations on 112,888 real and hypothetical metal-organic framework structures in order to calculate their CO_2 permeabilities and CO_2/N_2 selectivities. The CO_2/H_2O sorption selectivity of 2,017 real MOFs was evaluated using the H_2O sorption data of Li et al.[1] Using experimentally measured polymer properties and the Maxwell model, we predicted the properties of all of the hypothetical mixed matrix membranes that could be made by combining the metal-organic frameworks with each of nine polymers, resulting in over one million possible MMMs. The predicted gas permeation of MMMs was compared to published gas permeation data in order to validate the methodology. We then carried out twelve individually optimized techno-economic evaluations of a three-stage membrane-based capture process. For each evaluation, capture process variables such as flow rate, capture fraction, pressure and temperature conditions were optimized and the resultant cost data were interpolated in order to assign cost based on membrane selectivity and permeability. This work makes a connection from atomistic simulation all the way to techno-economic evaluation for a membrane-based carbon capture process. We find that a large number of possible mixed matrix membranes are predicted to yield a cost of carbon capture less than \$50 per tonne CO_2 removed, and a significant number of MOFs so identified have favorable CO_2/H_2O sorption selectivity.

Broader context

Emissions of CO_2 from coal power plants are a major contributor to the rise in greenhouse gases and, consequently, climate change. As part of a broader strategy to reduce greenhouse gas emissions, significant effort has been made to develop efficient CO_2 capture and storage technologies. These technologies can potentially be retrofitted onto existing coal power plants, where a portion of the produced power is diverted to operate the CO_2 capture process. However, many CO_2 capture technologies are cost prohibitive to operate because too much power would need to be diverted instead of sold to customers. Membranes that separate CO_2 from the other components of the gaseous exhaust stream have great potential as energy-efficient and low-cost solutions to this urgent problem. In particular, mixed matrix membranes, which are polymers containing well-dispersed small inorganic particles, offer the potential for much better performance than ordinary (i.e., pure polymer) membranes. There are many possible polymers, and many possible inorganic particles, from which to construct mixed matrix membranes, and it can be a challenge to find the optimal combination. In this work, we use computational modeling to rapidly screen mixed matrix membranes in order to estimate both their CO_2 capture performance and the resulting cost of carbon capture. A key finding of this work is the identification of a large number of hypothetical mixed matrix membranes that are predicted to yield a cost of carbon capture of less than \$50 per tonne of CO_2 removed.

1 Introduction

Anthropogenic emissions of CO_2 are key contributors to global climate change, and coal-fired power plants represent a large proportion of overall world-wide CO_2 emissions.[2] Researchers have long sought an economically viable method to separate and sequester the CO_2 generated by power production from coal, instead of releasing it into the atmosphere. The separation process differs depending on whether one considers post-combustion capture from flue gas or pre-combustion capture from gasified coal synthesis gas. Most of the energy produced from coal world-wide is currently generated in pulverized coal plants, where coal and air are combusted in a boiler.[2] A retrofitted carbon capture process for such a plant would be called a post-combustion process. Post-combustion separation is particularly challenging because CO_2 is at a low concentration ($\sim 13\%$) in the flue gas. While future power plants might benefit from pre-combustion carbon capture technologies, existing coal power plants will need retrofitted post-combustion technologies in order to significantly reduce carbon emissions.

CO_2 capture using amine solvents is a mature technology used for CO_2 separations in certain industrial processes,[3] but there are significant drawbacks to its application to post-combustion carbon capture. Techno-economic estimates for amine-based solvent processes show that such systems would be quite costly as well as face scale-up challenges.[4] A typical 600 MWe power plant can produce 500 m^3 of flue gas every second. Amine-based processes currently used for carbon dioxide separations in the natural gas and chemical industries treat gas streams that are five to ten times smaller.[5] For the case of post-combustion capture, emerging technologies such as cryogenic separation, precipitating solvents, sorbents, or membranes could prove to be far more effective and economical in the long run.[6]

Gas separations using polymer membranes are attracting interest for post-combustion carbon capture due to their low energy requirements, ease of fabrication, and excellent mechanical properties. Pure polymers, however, exhibit a tradeoff between selectivity and permeability, as was demonstrated by Robeson.[7,8] Known polymer membranes are either highly selective or highly permeable. The tradeoff between selectivity and permeability that has been identified for pure polymers is often referred to as the Robeson bound.

Mixed matrix membranes (MMM) are polymer membranes with inorganic nanoparticles dispersed in the polymer matrix. The polymer matrix contributes mechanical strength and ease of fabrication while the incorporation of certain inorganic particles can improve separation and permeation properties. Materials such as zeolites,[9] silica,[10], carbon molecular sieves[11] and metal-organic frameworks[12,13] have been incorporated into MMMs. Metal-organic frameworks (MOFs) are highly porous crystalline materials created via the self-assembly of inorganic metal or metal oxide subunits with organic linkers.[14–16] MOFs can be made from an enormous number of possible building blocks, leading to a material class encompassing a wide variety of properties.[17–19] The incorporation of certain CO_2/N_2 selective and highly permeable MOFs into polymers has been shown to increase selectivity and permeability of the MMM, with respect to the neat polymer,[12,20,21] although not all MOF-polymer pairings result in an improvement over the parent polymer. In this work, we have used computational methods to screen a large number of MOFs and predict the properties of possible MMMs. These computational methods have been pioneered by others,[23,30,32,33] but we have proceeded a step further by pushing our predictions into the process optimization and cost evaluation realms.

Due to the large number and variety of MOF structures and the difficulty involved in measuring gas permeation through MOFs, it is difficult to predict *a priori* which MOF should be paired with which polymer in order to produce a high-performing MMM. There are thousands of synthesized MOFs,[22] and an almost infinite number of possible MOFs that could be synthesized in the future.[23,24] There are on the order of a hundred polymers that have been used for separation membranes and by blending polymers together, an even larger number of polymer materials may be created. It would be an impossible feat to synthesize and ex-

a National Energy and Technology Laboratory, 626 Cochrans Mill Road, Pittsburgh, Pennsylvania 15236, USA.

b AECOM, 626 Cochrans Mill Road, Pittsburgh, PA 15236, USA. Fax: 41 2386 4604 ; Tel: 41 2386 7337; E-mail: samir.budhathoki@netl.doe.gov

c Department of Chemical and Petroleum Engineering, University of Pittsburgh, 3700 O'Hara St, Pittsburgh, Pennsylvania 15261, USA.; E-mail: wilmer@pitt.edu

perimentally test all the possible MMMs that could be created from this array of materials. Therefore, a high-throughput screening of computed MMM properties will be extremely useful in order to identify the relationship between the MOF properties, the polymer properties and the properties of the MMM. In this study, we have used computational methods to predict the gas permeability and selectivity of 112,888 MOFs, combined those data with experimentally-measured properties of nine polymers and, making use of the Maxwell model,[25] predicted the gas separation properties of over a million MMMs. Similar computational screening projects have been carried out previously, not only on MOFs,[1,23,24,26–29] but also on MMMs.[30–33] While computational screening projects have already yielded useful results, the question of how MOFs in MMMs will be affected by water remains an outstanding issue. In addition to CO_2 and N_2 sorption data, we made use of results obtained by Li et al.[1] for H_2O sorption in real MOFs (2,017) to judge whether MOFs in MMMs are CO_2/H_2O sorption selective or not. By separating a large group of MOFs into those that either are, or are not, CO_2/H_2O sorption selective, we have been able to show that there are a significant number of MOFs that show favorable CO_2/N_2 separation properties and are not sorption selective for water.

However, a further goal of our work is to understand how the properties of MMMs influences the cost of carbon capture. Typically, in order to do a techno-economic evaluation of a carbon capture process, the properties of the separation membrane are known and a capture process is designed to minimize the annualized cost. The design of a capture process includes process configuration as well as process variables. Both the process configuration and the variables in the carbon capture process (temperature, pressures, flow rates, the area of the membranes, etc.) may be optimized based on the properties of a material.[34] In this work, we have adopted a three-stage process configuration that has been demonstrated to be well-suited for membrane-based post-combustion carbon capture.[35] We have optimized the design and operating conditions for this process for twelve distinct selectivity-permeance conditions. By carrying out a linear interpolation over the selectivity and permeance ranges of interest, we created an estimate of the cost of carbon capture (CCC) as a function of membrane selectivity and permeance properties for the range of interest. We have used this relationship in order to create a database of over a million possible MMMs, each with an associated estimate for its CCC.

2 Computational methodology

2.1 Materials studied

We studied hypothetical MOFs from the database created by Wilmer et al.[23], and real MOFs included in the computational ready experimental (CoRE) MOF database created by Chung et al.[36] The hypothetical database contains 137,953 MOF structures systematically created by re-connecting a library of building blocks (gleaned from known MOFs). The CoRE database includes a collection of structurally and chemically diverse real MOFs that have been synthesized and experimentally characterized; during creation of the CoRE database the experimentally-obtained

structure files were altered in order to remove solvent molecules, resolve partial occupancies and remove disorder. Out of the 4764 structures in the CoRE database, we chose to focus on MOFs that would be characterized effectively using the automated methods and the EQeq partial charge assignment methodology applied in this project.[37] Thus we focused on MOFs with metal oxide subunits (as opposed to metal-metal bonds or uncommon oxidation states). We removed from our study group any MOFs with pore diameters less than 2 Å. We further excluded certain MOF structures from both the hypothetical and CoRE databases for which our simulations provided insufficiently reliable data (details are provided in the supplementary information). After excluding MOF structures as detailed above, our study group included >110,000 hypothetical and >2,000 CoRE MOFs.

In order to predict the properties of MMMs, we combined our computational results for MOFs with experimental data from nine polymer materials: poly[1-(trimethylsilyl)-1-propyne] (PTMSP),[38] poly[1-(trimethylgermyl)-1-propynel] (PTMGP),[38] polymers of intrinsic microporosity-1 (PIM-1),[39] polydimethylsiloxane (PDMS),[40] 2,6-diisopropylphenyl amino-hydroxy functionalized polydimethylsiloxane (modified PDMS),[41] polymers of intrinsic microporosity-7 (PIM-7),[42] 2,2'-bis(3,4'-dicarboxyphenyl) hexafluoropropane dianhydride- 2,3,5,6-tetramethyl-1,4-phenylenediamine (6FDA-durene),[43] poly[bis(2-(2-methoxyethoxy)ethoxy)]polyphosphazene (MEEP),[44] and 5(6) -1-(4'aminophenyl)-1,3,-trimethylindane (Matrimid-5218).[12] This group of polymers spans a wide range of CO_2 permeability and intentionally includes many of the polymers that have been previously used in the formulation of MMMs.

2.2 Structural characterization

Using the freely-available Zeo++ software,[45] we have calculated the pore limiting diameter (PLD), largest cavity diameter (LCD) and the dimensionality of the pores for each MOF. The PLD is the diameter of the largest sphere that can move through the structure without overlapping framework atoms and the LCD is defined as the diameter of the largest sphere that could be inserted into a cavity in the structure.[26]

2.3 Force field

An all-atom pairwise force field of the following functional form was used to describe the interactions between all the atoms in the system:

$$V_{tot} = \sum_{i=1}^{N-1} \sum_{i<j}^{N} \left\{ 4\varepsilon_{ij} \left[\left(\frac{\sigma_{ij}}{r_{ij}} \right)^{12} - \left(\frac{\sigma_{ij}}{r_{ij}} \right)^{6} \right] + \frac{q_i q_j}{4\pi\varepsilon_0 r_{ij}} \right\} \qquad (1)$$

where ε_{ij} and σ_{ij} are the well depth and collision diameters, r_{ij} is distance between the atoms i and j, q_i is the atomic charge of atom i, and $\varepsilon_0 = 8.8542 \times 10^{-12}$ C^2 N^{-1} m^{-2} is the permittivity of vacuum. Metal-organic framework atoms were held rigid. The atoms in the MOFs were described using Lennard Jones parameters from the universal force field (UFF)[46] and the partial charges were derived via the extended charge equilibration method (EQeq) developed by Wilmer and Snurr.[37] The TraPPE[47] force field was used

for CO_2 and N_2. The Lorentz Berthelot combining rules were used to calculate the Lennard Jones parameters for unlike atom pairs.

2.4 Widom particle insertion and molecular dynamics simulations

We performed atomistic simulations to characterize gas sorption and permeability in the MOFs. Because we have largely adopted the methodology of a number of previous works,[26,30,31] a detailed description has been placed in the supporting information and only a brief overview is presented here. We used the Widom particle insertion method,[48] as implemented in the RASPA[49] code in order to calculate the Henry's law constants (gas adsorption at low partial pressure) of CO_2 and N_2 of each MOF at 298 K. Henry's constants are frequently used in the literature to approximate gas adsorption at low partial pressures, where the approximation becomes exact only at infinite dilution. At higher pressures, using Henry's constants can lead to significant over prediction of adsorption. Furthermore, in large-scale screening studies that utilize method like Widom insertion, there is a significant chance that a small number of materials will be poorly sampled and for which calculated Henry's constants may be artificially high for statistical reasons. The self-diffusivities of CO_2 and N_2 in each MOF were computed using the molecular dynamics code LAMMPS[50] at 298 K. In order to account for the effect of water on gas permeability in MOFs, we have used the calculated H_2O adsorption data from Li et al.[1] to compute the CO_2/H_2O sorption selectivity for a majority of the MOFs in the CoRE database. MOFs in the CoRE database are categorized as CO_2/H_2O sorption selective or vice versa based on this result. The gas separation performance of porous materials may be described via a solution-diffusion mechanism in which the permeability of species i, P_i, is the product of the solubility, S_i, and the diffusivity, D_i. The perm-selectivity for species i over species j ($\alpha_{i/j}^{P}$), is thus:

$$\alpha_{i/j}^{p} = \frac{P_i}{P_j} = \alpha_{i/j}^{S} \times \alpha_{i/j}^{D} \qquad (2)$$

where the superscripts D and S denote diffusion and solubility, respectively. We made use of this relation in order to calculate the CO_2/N_2 selectivity for each MOF or MMM.

2.5 Mixed matrix membranes

The selectivity and permeability of a membrane can be improved or degraded by the incorporation of porous filler materials. The Maxwell-Wagner-Sillars equation was derived in order to predict the dielectric behavior of composite materials, and the analogy between dielectrics and the permeation of gases through composite membrane materials was described by Bouma et al.[51] With the assumption that the filler particles are spherical, the Maxwell-Wagner-Sillars equation simplifies to Eq. 3 and the model is commonly referred to as the "Maxwell model".

$$P_{MMM} = P_{poly} \frac{P_{MOF}(1 + 2\phi_{MOF}) + P_{poly}(2 - 2\phi_{MOF})}{P_{MOF}(1 - \phi_{MOF}) + P_{poly}(2 + \phi_{MOF})} \qquad (3)$$

where P_{MMM} is the effective permeability of the composite MMM material, P_{poly} is the permeability of the neat polymer, and P_{MOF}

is the permeability of the MOF filler particles, respectively. ϕ_{MOF} is the volume fraction of the MOF filler particles, for which we have assumed a value of 0.30 (which is in line with the volume fractions adopted in MMM materials that have been synthesized). The Maxwell model assumes that the flux of gas around and through the MOF particles is not influenced by neighboring particles. This assumption limits the applicability of the Maxwell model to volume fractions of 0.30 or less. Despite these simplifying assumptions, this model has been shown to be quite successful in a number of previously published works.[31,32,52–55] We compare the predictions made in this work with published measurements of CO_2 and N_2 permeation in MMMs (Figure 4), and we find that our predictions are in overall good agreement with the experiments.

We use our calculated data on gas permeation through the MOFs, and we make use of experimentally determined data (presented in the supporting information) for the neat polymer membranes. Thus, we are able to make predictions of gas permeability for one hypothetical MMM for each combination of the 112,888 MOFs and 9 polymers included in our study, yielding predictions for over one million MMMs. By predicting both the CO_2 and the N_2 permeability, we are able to calculate the ideal CO_2/N_2 selectivity using Eq. 2. In order to bridge the gap from the material to the process, we assume that each MMM may be incorporated as a one micron thick selective layer on a porous support as part of a gas separation membrane module, yielding a predicted permeance for each MMM.

2.6 Process modelling

We have used a process model in order to link our results from atomistic simulations to estimates for the cost of carbon capture.[56,57] The goal of our techno-economic calculations is to understand how membrane-based post-combustion carbon capture process costs are related to the properties of the membrane. The calculations are based on capturing 90% of the CO_2 from a 650 MWe supercritical pulverized coal power plant. In this work, we have assumed a price of $50/m^2 for the cost of the separation membrane modules, in line with numerous previous studies.[58–61] Module fabrication costs will include raw material cost, support and dense layer fabrication, and module fabrication complete with fittings. The cost of material, therefore, is to some extent dwarfed by the manufacturing costs. As with any new technology, the cost of a material will decrease sharply over time if there is robust demand. This has been observed in the market as MOF materials have made their way into products.[62] The optimizations were performed within the Framework for Optimization, Quantification of Uncertainty and Sensitivity (FOQUS), utilizing Aspen Custom Modeler to simulate the membrane-based carbon capture process and a spreadsheet for calculating the capital and operating costs to enable estimation of the cost of electricity. For a post-combustion carbon capture technology, the flue gas has been subjected to pre-treatment to reduce SO_x and NO_x prior to entering the membrane carbon capture unit. The cost of SO_x and NO_x removal makes up part of the total overnight cost of the power plant and was thus included in the costing formula.

We assumed a three-stage process configuration with sweep that is a variant of a design published by Merkel et al.[5] The configuration introduced by Merkel et al. includes a sweep gas stream to recycle CO_2-rich permeate to the boiler, to increase the driving forces across the membrane. Within the NETL variant, the retentate stream from the third stage is redirected into the second stage to avoid dilution of the stream entering the first stage. Our goal was to estimate a cost for carbon capture for any of the hypothetical membranes in our large data set. Usually, one would design an entire carbon capture process based on the specific properties of a given membrane, optimizing everything about the process in order to determine the lowest cost for a process designed for that membrane. In this work, however, we created an optimized process for twelve hypothetical membranes characterized by their selectivity and permeance. The chosen three-stage process configuration was not varied. The twelve hypothetical membranes were characterized by CO_2 permeance equal to 34, 1170 or 8000 GPU and CO_2/N_2 selectivity of 18, 35, 68 or 250. For each permeance-selectivity pair, membrane area, pressures, temperatures and flowrates were optimized in order to minimize the cost of electricity. Using those data, a linear interpolation was applied in order to create a relationship between the cost of carbon capture and the permeance (P_{CO_2}) and selectivity (α_{CO_2/N_2}^P) of the membrane (Eq. 4)

$$CCC\left(\frac{\$}{tonne\ CO_2\ removed}\right) = f\left(P_{CO_2}, \alpha_{CO_2/N_2}^P\right) \qquad (4)$$

Ultimately, we have assigned a predicted CCC to each hypothetical MMM in our database based on the selectivity and permeance of the MMM. Further details of the process modelling may be found in the supplementary information.

3 Results and discussion

3.1 Gas adsorption in metal-organic frameworks

The calculated Henry's constants for CO_2 and N_2 as a function of LCD are shown in Figure 1. Results are shown for MOFs from the hypothetical database as well as from the CoRE database. Several well-known MOFs are highlighted for comparison. The Henry's constants of CO_2 are typically an order of magnitude larger than those of N_2, as would be expected due to the stronger electrostatic forces that dominate the CO_2-MOF atom interactions. The Henry's constants for both gases show a peak near LCD 4-6 Å, indicating that pores in that size range accommodate the gas molecules in regions of space where favorable interactions with framework atoms are most likely.

The CO_2/N_2 ideal adsorption selectivities for the MOFs were computed from the ratio of their corresponding Henry's constants and are presented as a function of LCD in Figure 1c. It can be seen that adsorption selectivity is greater than one for all the MOFs, due to the fact that the CO_2-MOF interaction benefits from a larger electrostatic interaction than the N_2-MOF interaction. It is also observed that the MOFs with the largest adsorption selectivity are those with LCD $\sim$ 4-6 Å. Out of the six well-known MOFs highlighted, SIFSIXCu2i has the largest adsorption selectivity (α_{CO_2/N_2}^S) of 271.

3.2 Diffusion of CO_2 and N_2 in metal-organic frameworks

The self-diffusion coefficients of CO_2 and N_2 in MOF materials were computed from molecular dynamics trajectories and, in general, the self-diffusivities tend to increase with pore size. (Details are presented in the supporting information.) The LCD/PLD ratio is an indication of the morphology of a MOF; a ratio of 1 indicates the cavities in the MOF are similar in size to the channels, while a ratio greater than one indicates that the MOF has large cavities connected by narrow channels.[63] We examined the relationship between self-diffusivity of gases in MOFs and the LCD/PLD ratio, and the results are presented in Figure 2. MOF morphology has a strong effect on diffusivity. Diffusion for both gases is enhanced when the LCD/PLD ratio is between 1 and 2, indicating that gas diffusivity is enhanced when the cavities are similar in size to the channels. MOFs with large LCD/PLD ratios (that contain relatively large cavities connected by narrow channels) allow for limited gas diffusivity, indicating that gas molecules spend a lot of time in large cavities and may have difficulty escaping through narrow channels. In Figure 2 (c), we present CO_2/N_2 diffusion selectivity as a function of PLD. It can be seen that many of the MOFs that have PLD < 5 Å show high diffusion selectivity. Conversely, MOFs with large PLD do not tend to show high CO_2/N_2 selectivity. In general, when the PLD is large, diffusion of gases is less influenced by the chemical environment of the pore walls and selectivity is lost. $\sim$ 70% of the hypothetical MOFs and $\sim$ 50% of the CoRE MOFs have CO_2/N_2 diffusion selectivity less than one; e.g. they are selective for N_2 rather than CO_2. This includes also the popular MOFs Cu-BTC, IRMOF-1 and IRMOF-3. This may be attributed to the stronger MOF-CO_2 interaction and greater molar mass of CO_2 compared to N_2. In Figure 3, we present the CO_2/N_2 selectivity as a function of CO_2 permeability for the MOFs we have studied. These results, in agreement with previous studies,[28,31,32] confirm that there are a large number of MOF materials that greatly exceed the Robeson bound.

3.3 Mixed matrix membranes

We predicted the properties of composite membranes using computed data for CO_2 and N_2 permeabilities in the MOFs and experimentally measured gas permeabilities in nine polymers. The permeability of the gases in the composite material was computed by means of the Maxwell model. In order to assess the reliability of this method, we have compared our predictions with experimental measurements for a series of MMMs (Figure 4).[13,64–70] It can be seen that our predictions for CO_2 and N_2 permeability are reasonably close to the measured values.

In Figure 5, we present the calculated selectivity and CO_2 permeability for the MMMs. For each polymer, the properties of the neat polymer membrane are marked with a square and the predicted properties for MMMs derived from that polymer are marked with smaller symbols in the same color. Based on these results, the incorporation of MOFs into polymer membranes can either improve or degrade performance. It can be seen that for both the CoRE and hypothetical databases, there are a large number of MOFs which, in combination with highly permeable polymers, could lead to the creation of MMMs that greatly exceed the Robe-
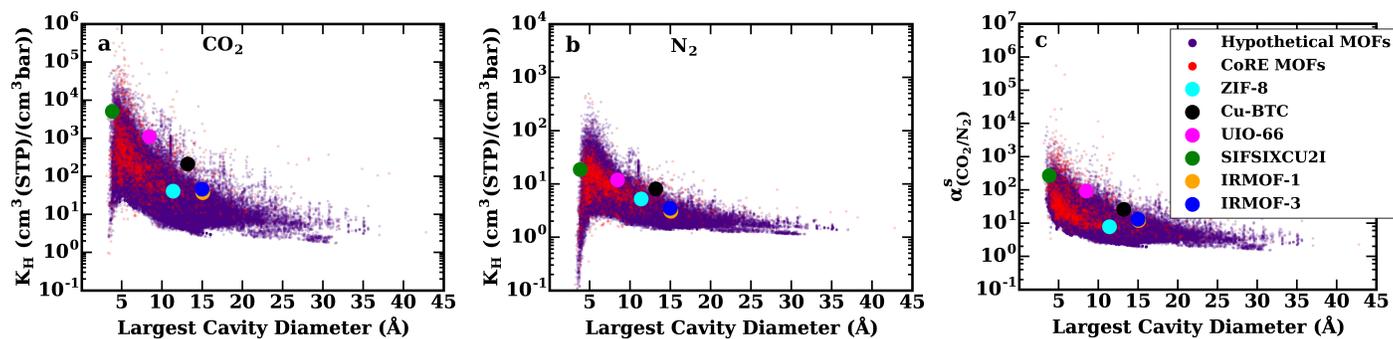
Fig. 1 Calculated Henry's constants for CO_2 (a), N_2 (b) and ideal CO_2/N_2 selectivity (c) as a function of largest cavity diameter (LCD) in metal-organic frameworks. Hypothetical MOFs are indicated with purple dots and MOFs from CoRE database are idicated with red dots.
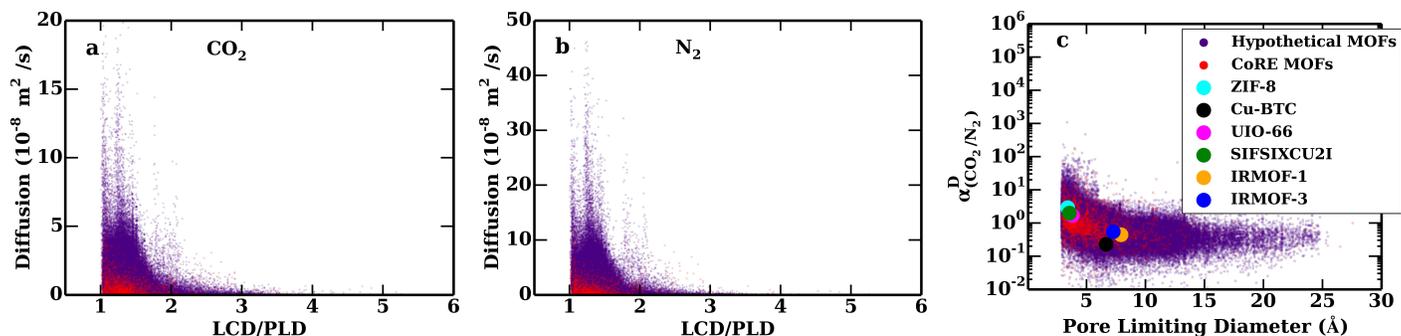
Fig. 2 Self-diffusion coefficients of CO_2 (a) and N_2 (b) in MOFs as a function of pore morphology (LCD/PLD) and CO_2/N_2 Diffusion selectivity (c) as a function of Pore Limiting Diameter (PLD) at 298 K. Diffusion for CO_2 and N_2 have been cut off at 20 ($10^{-8} m^2/s$) and 50 ($10^{-8} m^2/s$) for clarity.
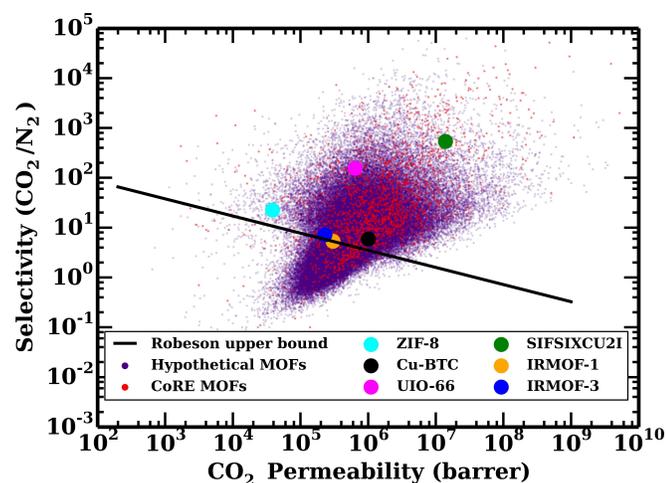
Fig. 3 CO_2/N_2 selectivity as a function of CO_2 permeability for hypothetical and CoRE MOFs. The black diagonal line indicates the Robeson upper bound.

Fig. 4 Predicted versus measured CO_2 and N_2 permeabilities of mixed matrix membranes using Maxwell model with the experimental values. Blue color represents CO_2 permeability and green color represents N_2 permeability. The red diagonal line indicates calculated permeability = experimental permeability.

son bound. The largest impacts are seen for the most highly permeable polymers. It is observed that MMMs made with low permeability polymers such as Matrimid are unlikely to exceed the Robeson bound.

The influence of MOF permeability on MMM permeability is examined in Figure 6. In this figure, the CO_2 permeability of the MMM is plotted as a function of the ratio of the MOF permeability over the neat polymer permeability. When the MOF permeability is less than the neat polymer permeability, the MMM permeabil-

ity is less than that of the neat polymer. When the MOF permeability is greater than that of the neat polymer, we see that the MMM permeability improves. However as the ratio continues to increase, the MMM CO_2 permeability levels off and no longer increases. This leveling off is complete by the time the MOF permeability is approximately 10 times that of the polymer. It has been previously noted that predictions based on the Maxwell model
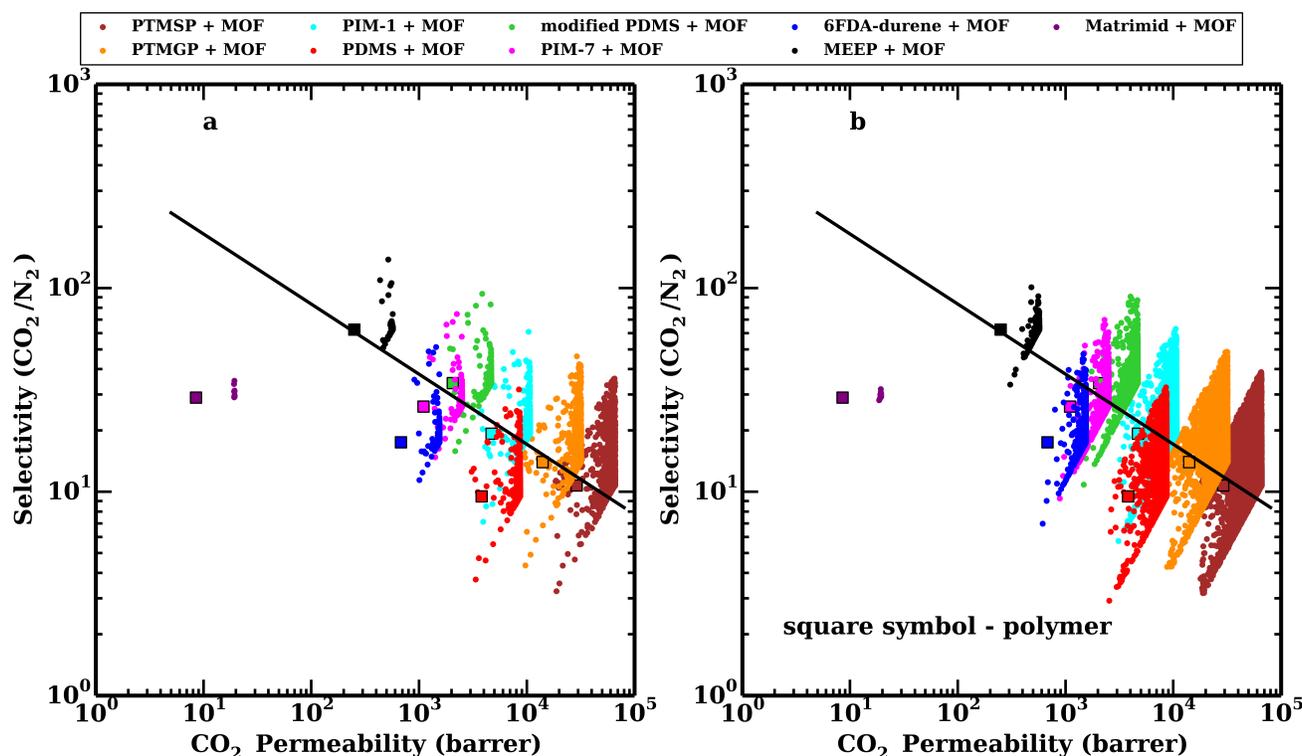
Fig. 5 Selectivity as a function of CO_2 permeability for MMMs based on a) the CoRE database of Chung et al.[36] and b) the hypothetical MOF database of Wilmer et al.[23] The diagonal line is the Robeson bound. The square symbols mark the selectivity and permeability of the neat polymers and the small round symbols mark the predicted selectivity and permeability of the MMMs based on each of the nine polymers.

show that MMMs may be improved by the incorporation of highly porous MOF filler particles up to a point,[51] after which there is no further improvement. From the Maxwell model, one can compute the maximum and minimum theoretically achievable limits to the MMM permeability, which are 2.285 and 0.608 times that of the polymer, respectively. This underscores the importance of choosing a highly permeable polymer to start with. To achieve a MMM with the highest possible CO_2 permeability, one should begin with a polymer with the highest possible permeability and pick a MOF with permeability that is at least 10 times that of the neat polymer.

We also can explore how the relationship between MOF and polymer selectivity influences the MMM selectivity. This relationship is presented in Figure 7 for four fixed ratios of MOF/polymer permeability: 1, 10, 100 and 10,000. When the MOF selectivity is less than that of the polymer, the MMM selectivity is poor. As the MOF selectivity is increased relative to that of the polymer, the MMM selectivity increases as well, before eventually leveling off. The MMM in which the MOF/polymer permeability ratio is 1 does not reach a high selectivity. The MMMs for which the ratios are greater than 10 both reach the same maximum selectivity, but the MMM for which the ratio is 100 hits the maximum selectivity sooner. In the case where the MOF/polymer permeability ratio is 100, the maximum MMM selectivity is reached when the MOF selectivity is about 1000 times that of the polymer selectivity. Therefore, to achieve the highest selectivity and permeability in a MMM, which should begin with a polymer with high permeability, pair it with a MOF with at least 100 times more permeability

and 1000 times higher selectivity.
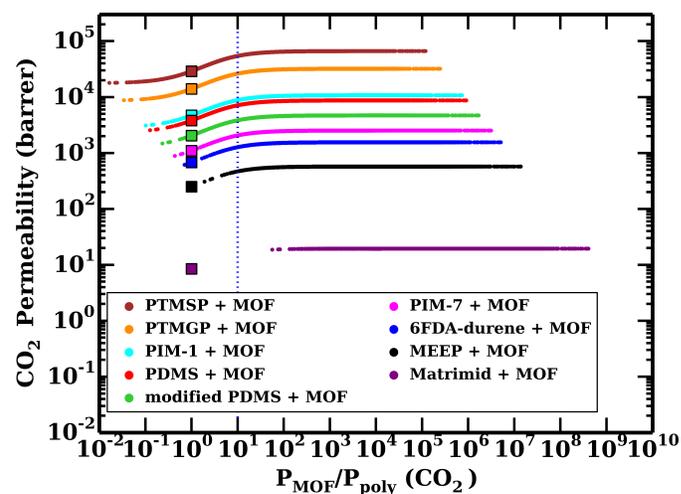
Fig. 6 MMM CO_2 permeabilty as a function of the ratio of the MOF permeability over the polymer permeability. Square symbols are CO_2 permeability values of pure polymers.

3.4 Cost of carbon capture

In Figure 8, we present results for the cost of carbon capture for MMMs that could be made from the hypothetical MOF database and PIM-1. The permeability and selectivity of the neat membrane is labelled with a dark diamond. MOFs with permeability or selectivity lower than that of the neat membrane are predicted
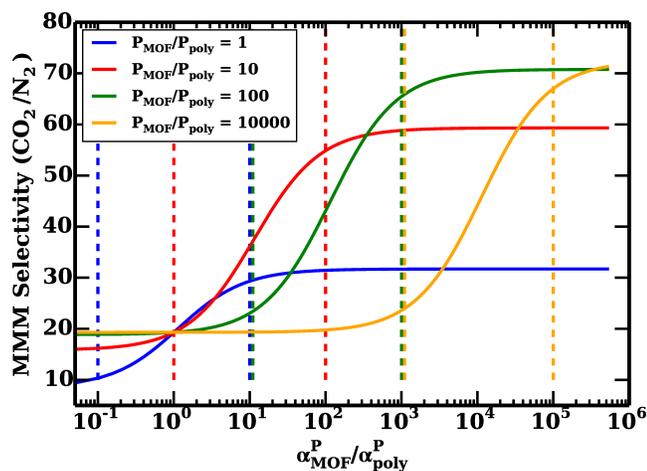
Fig. 7 Relationship between gas selectivity of mixed membranes and the ratio of gas permeability and gas selectivity of MOF to polymer. This figure is based on the PIM-1 which has a selectivity of 19.3. The colored dashed lines show the regions where MMM selectivity is increased for each given ratio of MOF to polymer permeability. It is observed that for a given MOF to polymer permeability ratio, MMM selectivity starts increasing once the MOF to polymer selectivity ratio approaches $0.1*P_{MOF}/P_{poly}$ and levels off around $10*P_{MOF}/P_{poly}$.

Fig. 8 Selectivity as a function of CO_2 permeability for the hypothetical MOF database. Color denotes the predicted CCC for MMM generated with the MOF and PIM-1.

to lead to MMMs with high CCC. In fact, the pure polymer outperforms a significant number of possible MMMs, underscoring the importance of pairing a polymer with a MOF that has the right properties in order to get an MMM with superior qualities. It can be seen that MOFs leading to membranes predicted to have the best CCC have CO_2 permeability about 100 times that of the polymer and CO_2/N_2 selectivity roughly 1000 times larger than those of the neat polymer. This is consistent with the results presented in the previous section. It is interesting that the lowest CCC is not yielded by the "best" MOF, e.g. the MOF with the highest permeability or the selectivity. In fact what is revealed is that the relationship between the polymer and the MOF is more important than the properties of the MOF alone. As shown in Figure 7, MOF/polymer selectivity ratio should not be less than one order of magnitude than MOF/polymer pemeability ratio in order for resulting MMM to show enhanced gas selectivity. Therefore, the lowest CCC is not shown by MOFs with the largest permeability and selectivity, but by those MOFs for which the MOF/polymer selectivity ratio is at least 10 times greater than the MOF/polymer permeability ratio, given the MOFs have larger permeability and selectivity compared to the polymer. These results highlight the importance placed on the choice of MOF when creating a MMM. While it is possible to improve the polymer properties by the incorporation of MOFs as filler particles, the choice of the wrong MOF can lead to a suboptimal result. In Figure 9a, we present results for MMMs based on CO_2/H_2O sorption selective MOFs from the CoRE MOF database and PIM-1. In Figure 9b, we present similar results for the H_2O/CO_2 sorption selective MOFs from the CoRE MOF database and PIM-1. Out of 2017 CoRE MOFs, the majority (1121) are CO_2/H_2O sorption selective and the minority (896) are selectively adsorbing H_2O over CO_2.

The CO_2/N_2 selectivity of the MMM is plotted as a function of CO_2 permeance, and the color of the background indicates the pre-

dicted CCC. The performance of neat PIM-1 membrane is marked with a diamond, and is predicted to give a CCC of $64 per tonne CO_2 removed.
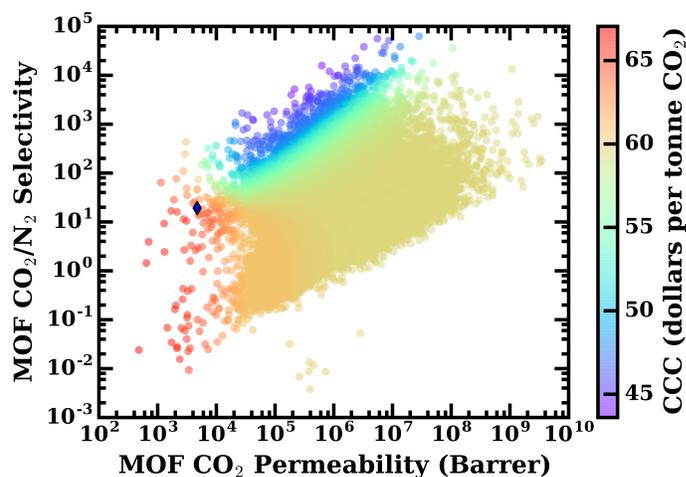
In total, our predictions include 1,153 hypothetical MMMs with predicted CCC less than $50 per tonne CO_2 removed. These membranes are based on modified PDMS (7), PDMS (1), PIM-1 (448), PTMGP (504) and PTMSP (193). Sixteen of these possible MMMs are notable because they are based on MOFs from the CoRE database with favorable CO_2/H_2O sorption selectivities. In these MOFs, the Henry's coefficient for CO_2 is 5 to 33 times larger than the Henry's coefficient for H_2O, giving some indication that these possible membranes could be robust in performance in a humid gas stream. Seven of these membranes are based on PIM-1 and are predicted to have CO_2 permeabilities of 7,000 to 11,600 Barrer and selectivities of 38-61. Membranes with properties in this range have not been previously reported. It is clear that the creation of MMMs with properties as described above would represent a major step forward in terms of materials discovery for membrane-based carbon capture processes.

4 Conclusions

In this work, we used simulations to predict the properties of a large number of hypothetical and existing MOFs. By means of the Maxwell model and the use of experimental data for nine polymers, we predicted the properties of ~1 million MMMs. Techno-economic evaluations of an optimized membrane-based capture process allowed us to develop a predicted CCC as a function of membrane CO_2 permeability and CO_2/N_2 permselectivity. Capture process variables such as flow rate, capture fraction, pressure and temperature conditions were optimized as a function of membrane properties. We have created a database of ~ 1 million hypothetical MMMs, each with a predicted cost of carbon capture. This work represents a novel connection between atomistic MOF structure and cost of carbon capture. Our calculations show that MOFs with LCD in the range of 4-10 Å and PLD in the range of 4-5 Å have superior adsorption and diffusion selectivity, respectively. In order to create a MMM with properties that greatly exceed
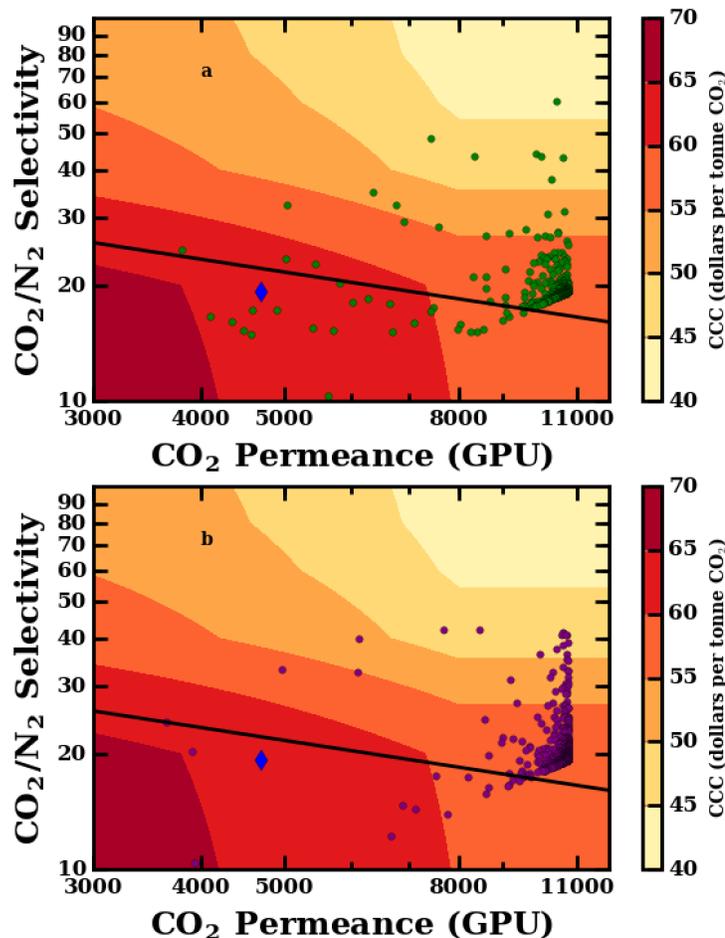
Fig. 9 (a) Performance of MMMs formed from CO_2/H_2O sorption selective CoRE MOFs and PIM-1. (b) Performance of MMMs formed from H_2O/CO_2 sorption selective CoRE MOFs and PIM-1. The performance of a membrane composed of neat PIM-1 ($64 per tonne CO_2 removed) is indicated by the location of the blue diamond. The Robeson upper bound is indicated by the a black line.

those of the parent polymer, the chosen MOF should have permeability roughly 100 times and selectivity roughly 1000 times greater than the polymer. Through techno economic analyses of ~ 1 million mixed matrix membranes, we found 1,153 MMMs that yield a CCC less than $50 per tonne CO_2 removed.

5   Acknowledgments

Disclaimer

Conflict of interest

There are no conflicts to declare.

References

1 S. Li, Y. G. Chung and R. Q. Snurr, *Langmuir*, 2016, **32**, 10368–10376.

2 R. K. Pachauri and L. Mayer, *Climate change 2014: synthesis report,* Intergovernmental panel on climate change fifth assessment report of the intergovernmental panel on climate change, 2015.

3 T. G. Rochelle, *Science*, 2009, **325**, 1652–1654.

4 M. R. Abu-Zahra, L. H. Schneiders, J. P. Niederer, P. H. Feron and G. F. Versteeg, *Int. J. Greenhouse Gas Control*, 2007, **1**, 37–46.

5 T. C. Merkel, H. Lin, X. Wei and R. Baker, *J. Membr. Sci.*, 2010, **359**, 126–139.

6 M. M. Abu-Khader, *Energy Sources Part A*, 2006, **28**, 1261–1279.

7 L. M. Robeson, *J. Membr. Sci.*, 1991, 165–185.

8 L. M. Robeson, *J. Membr. Sci.*, 2008, **320**, 390–400.

9 D. Bastani, N. Esmaeili and M. Asadollahi, *J Ind. Chem. Eng.*, 2013, **19**, 375–393.

10 B. Zornoza, S. Irusta, C. Téllez and J. Coronas, *Langmuir*, 2009, **25**, 5903–5909.

11 D. Q. Vu, W. J. Koros and S. J. Miller, *J. Membr. Sci.*, 2003, **211**, 311–334.

12 S. R. Venna, M. Lartey, T. Li, A. Spore, S. Kumar, H. B. Nulwala, D. R. Luebke, N. L. Rosi and E. Albenze, *Journal of Materials Chemistry A*, 2015, **3**, 5014–5022.

13 E. V. Perez, K. J. Balkus, J. P. Ferraris and I. H. Musselman, *J. Membr. Sci.*, 2009, **328**, 165–173.

14 Hailian Li and Eddaoudi, *Nature*, 1999, **402**, 276.

15 M. Eddaoudi, J. Kim, J. B. Wachter, H. K. Chae, M. O'Keeffe and O. M. Yaghi, *J. Am. Chem. Soc.*, 2001, **123**, 4368–4369.

16 M. E. Braun, C. D. Steffek, J. Kim, P. G. Rasmussen and O. M. Yaghi, *Chem. Commun.*, 2001, **0**, 2532–2533.

17 M. Eddaoudi, D. B. Moler, H. Li, B. Chen, T. M. Reineke, M. O'Keeffe and O. M. Yaghi, *Acc. Chem. Res.*, 2001, **34**, 319–330.

18 G. Lu, S. Li, Z. Guo, O. K. Farha, B. G. Hauser, X. Qi, Y. Wang, X. Wang, S. Han, X. Liu, J. S. DuChene, H. Zhang, Q. Zhang, X. Chen, J. Ma, S. C. J. Loo, W. D. Wei, Y. Yang, J. T. Hupp

and F. Huo, *Nat. Chem.*, 2012, **4**, 310–316.

19   J. Bonnefoy, A. Legrand, E. A. Quadrelli, J. Canivet and D. Farusseng, *J. Am. Chem. Soc.*, 2015, **137**, 9409–9416.

20   S. Zhao, X. Cao, Z. Ma, Z. Wang, Z. Qiao and S. Wang, Jixiao an d Wang, *Ind. Eng. Chem. Res.*, 2015, **54**, 5139–5148.

21   S. Basu, A. Cano-Odena and I. F. J. Vankelecom, *Sep. Purif. Technol.*, 2011, **81**, 31–40.

22   C. R. Groom, I. J. Bruno, M. P. Lightfoot and S. C. Ward, *Acta Cryst.*, 2016, **72**, 171–179.

23   C. E. Wilmer, M. Leaf, C. Y. Lee, O. K. Farha, B. G. Hauser, J. T. Hupp and R. Q. Snurr, *Nat. Chem.*, 2011, **4**, 83–89.

24   M. Z. Aghaji, M. Fernandez, P. G. Boyd, T. D. Daff and T. K. Woo, *Eur. J. Inorg. Chem.*, 2016, **2016**, 4505–4511.

25   J. C. Maxwell, *Treatise on Electricity and Magnetism*, Oxford University Press, London, 1873.

26   E. Haldoupis, S. Nair and D. S. Sholl, *J. Am. Chem. Soc.*, 2010, **132**, 7528–7539.

27   E. Haldoupis, S. Nair and D. S. Sholl, *J. Am. Chem. Soc.*, 2012, **134**, 4313–4323.

28   T. Watanabe and D. S. Sholl, *Langmuir*, 2012, **28**, 14114–14128.

29   N. S. Bobbitt, J. Chen and R. Q. Snurr, *The journal of Physical Chemistry C*, 2016, **120**, 27328–27341.

30   S. Keskin and D. S. Sholl, *Energy. Environ. Sci.*, 2010, **3**, 343–351.

31   Z. Sumer and S. Keskin, *J. Nanomater.*, 2016, **2016**, 1–12.

32   I. Erucar and S. Keskin, *J. Membr. Sci.*, 2012, **s 407-408**, 221–230.

33   I. Erucar and S. Keskin, *Ind. Eng. Chem. Res.*, 2011, **50**, 12606–12616.

34   A. Skorek-Osikowska, u. Bartela and J. Kotowicz, *Applied Energy*, 2017, **200**, 73–88.

35   O. Ajayi, *under preparation*, 2017.

36   Y. G. Chung, J. Camp, M. Haranczyk, B. J. Sikora, W. Bury, V. Krungleviciute, T. Yildirim, O. K. Farha, D. S. Sholl and R. Q. Snurr, *Chem. Mater.*, 2014, **26**, 6185–6192.

37   C. E. Wilmer and R. Q. Snurr, *Chem. Eng. J.*, 2011, **171**, 775–781.

38   T. Mizumoto, T. Masuda and T. Higashimura, *J. Polym. Sci. A Polym. Chem.*, 1993, **31**, 2555–2561.

39   A. K. Sekizkardes, V. A. Kusuma, G. Dahe, E. A. Roth, L. J. Hill, A. Marti, M. Macala, S. R. Venna and D. Hopkinson, *Chem-Comm.*, 2016, **52**, 11768–11771.

40   T. C. Merkel, V. I. Bondar, K. Nagai, B. D. Freeman and I. Pinnau, *J. Polym. Sci. B Polym. Phys.*, 2000, **38**, 415–434.

41   U. Senthilkumar and B. S. R. Reddy, *J. Membr. Sci.*, 2007, **292**, 72–79.

42   P. M. Budd, K. J. Msayib, C. E. Tattershall, B. S. Ghanem, K. J. Reynolds, N. B. McKeown and D. Fritsch, *J. Membr. Sci.*, 2005, **251**, 263–269.

43   W.-H. Lin and T.-S. Chung, *J. Membr. Sci.*, 2001, **186**, 183–193.

44   C. J. Orme, M. K. Harrup, T. A. Luther, R. P. Lash, K. S. Houston, D. H. Weinkauf and F. F. Stewart, *J. Membr. Sci.*, 2001, **186**, 249–256.

45   T. F. Willems, C. H. Rycroft, M. Kazi, J. C. Meza and M. Haranczyk, *Microporous Mesoporous Mater.*, 2012, **149**, 134–141.

46   A. K. Rappe, C. J. Casewit, K. S. Colwell, W. A. Goddard and W. M. Skiff, *J. Am. Chem. Soc.*, 1992, **114**, 10024–10035.

47   J. J. Potoff and J. I. Siepmann, *AIChE J.*, 2001, **47**, 1676–1682.

48   W. B., *J. Am. Chem. Soc.*, 1963, **39**, 2808–2812.

49   D. Dubbeldam, S. Calero, D. E. Ellis and R. Q. Snurr, *Mol Simul.*, 2016, **42**, 81–101.

50   S. Plimpton, *J. Comput. Phys.*, 1995, **117**, 1–19.

51   R. H. B. Bouma, A. Checchetti, G. Chidichimo and E. Drioli, *J. Membr. Sci.*, 1997, **128**, 141–149.

52   C. Altintas and S. Keskin, *Mol Simul.*, 2015, **41**, 1396–1408.

53   R. Mahajan and W. J. Koros, *Ind. Eng. Chem. Res.*, 2000, **39**, 2692–2696.

54   J. P. Boom, I. G. M. Pünt, H. Zwijnenberg, R. de Boer, D. Bargeman, C. A. Smolders and H. Strathmann, *J. Membr. Sci.*, 1998, **138**, 237–258.

55   J.-M. Duval, A. J. B. Kemperman, B. Folkers, M. H. V. Mulder, G. Desgrandchamps and C. A. Smolders, *J. Appl. Polym. Sci.*, 1994, **54**, 409–418.

56   J. Morinelly and D. Miller, *Post-combustion gas permeation carbon capture system models, AIChE Annual Meeting*, 2012.

57   J. Morinelly and D. Miller, *Gas permeation carbon capture — Process modeling and optimization, International Pittsburgh Coal Conference*, 2011.

58   A. Alshehri, R. Khalilpour, A. Abbas and Z. Lai, *Energy Procedia*, 2013, **37**, 976–985.

59   P. Shao, M. M. Dal-Cin, M. D. Guiver and A. Kumar, *J. Membr. Sci.*, 2013, **427**, 451–459.

60   N. C. Mat and G. G. Lipscomb, *Int. J. Greenhouse Gas Control*, 2017, **62**, 1–12.

61   H. Zhai and E. S. Rubin, *Environ. Sci. Technol.*, 2013, **47**, 3006–3014.

62   A. Scott, *Semiconductor industry to begin using MOFs | August 7, 2017 Issue - Vol. 95 Issue 32 | Chemical & Engineering News*, https://cen.acs.org/articles/95/i32/Semiconductor-industry-begin-using-MOFs.html.

63   B. J. Sikora, C. E. Wilmer, M. L. Greenfield and R. Q. Snurr, *Chem. Sci.*, 2012, **3**, 2217.

64   D. Eiras, Y. Labreche and L. A. Pessan, *Materials Research*, 2016, **19**, 220–228.

65   A. Car, C. Stropnik and K.-V. Peinemann, *Desal.*, 2006, **200**, 424–426.

66   B. Zornoza, B. Seoane, J. M. Zamaro, C. Téllez and J. Coronas, *ChemPhysChem*, 2011, **12**, 2781–2785.

67   S. R. Venna, A. Spore, Z. Tian, A. M. Marti, E. J. Albenze, H. B. Nulwala, N. L. Rosi, D. R. Luebke, D. P. Hopkinson and H. R. Allcock, *J. Membr. Sci.*, 2017, **535**, 103–112.

68   V. Nafisi and M.-B. Hägg, *Sep. Purif. Technol.*, 2014, **459**, 31–

38.

69 A. F. Bushell, M. P. Attfield, C. R. Mason, P. M. Budd, Y. Yampolskii, L. S. kova, A. Rebrov, F. Bazzarelli, P. Bernardo, J. C. Jansen, M. Lanč, K. Friess, V. Shantarovich, V. Gustov and

V. Isaeva, *J. Membr. Sci.*, 2013, **427**, 48–62.

70 Y.-S. Bae, J. Liu, C. E. Wilmer, H. Sun, A. N. Dickey, M. B. Kim, A. e. I. Benin, R. R. Willis, D. Barpaga, M. D. LeVan and R. Q. Snurr, *Chem. Commun.*, 2014, **50**, 3296–3298.